A re-assessment of aerosol size distributions from Masaya volcano (Nicaragua)

- R.S. Martin[ab]
- E. Ilyinskay[c]
- G.M. Sawyer[c]
- V.I. Tsanev[c],
- C. Oppenheimer[cde]

- [a] Department of Earth Sciences, University of Cambridge, UK
- [b] School of Biological and Chemical Sciences, Queen Mary, University of London, UK
- [c] Department of Geography, University of Cambridge, UK
- [d] Le Studium, Institute for Advanced Studies, Orleans and Tours, France
- [e] Institut des Sciences de la Terre d'Orléans, 1a rue de la Férollerie, 45071 Orléans, Cedex 2, France

Abstract

Cascade impactors were used to sample volcanic aerosol from Masaya (Nicaragua) in 2007, 2009 and 2010. Differences were found in the size distributions of volcanic aerosol between these recent campaigns and with a campaign in 2001: (1) SO_4^{2-} showed modes in both the fine (<1 μm; with low Na^+/K^+) and coarse (>1 μm; with high Na^+/K^+) fractions in all of the recent campaigns despite being unimodal in 2001 (<1 μm); (2) The modal diameters for SO_4^{2-} roughly doubled in 2009, compared to 2007 or 2010; (3) total Cl^- was depleted in volcanic aerosol compared to background aerosol in all the more recent campaigns but was enriched in 2001. Other aspects of the volcanic aerosol appear to be persistent, such as a fine SO_4^{2-}–H^+–Na^+–K^+ mode, which was the most abundant mode in all campaigns, and a coarse Cl^-–F^-–Mg^{2+}–Ca^{2+} mode of lower abundance. Water uptake and speciation in the aerosol were investigated using the equilibrium model, ISORROPIA II. Results show that the coarse SO_4^{2-}-rich mode deliquesces at lower relative humidity (40% RH) than the fine SO_4^{2-}-rich mode (50% RH) due to increased Na^+/K^+ in the former. The aerosol was predicted to be dry at ambient relative humidity in 2009 and dominated by $NaHSO_4$, $KHSO_4$, $CaSO_4$ and $MgSO_4$. In contrast, model results predict a liquid aerosol at ambient relative humidity in 2010. These results indicate that aerosol emissions from a volcano can vary in ionic composition and even more so in physical speciation (i.e., salts or solutions). These observations are set against a near-constant magmatic gas composition at Masaya, which highlights the significance of atmospheric and dynamic factors in the formation of volcanic aerosols.

Keywords : Masaya; Volcanic; Aerosol; Cascade impactor

1. Aerosol emissions from quiescently degassing volcanoes

Active volcanoes are a major natural source of aerosol to the atmosphere and their contribution to the aerosol burden is amplified by the typically high altitude of emission (Graf et al., 1997). The impacts of volcanic aerosol are most evident following large explosive eruptions (e.g., those of Krakatau in 1883 and Mt Pinatubo in 1991), when enormous quantities of fine ash and secondary sulphate aerosol are emplaced in the troposphere and

stratosphere. Such explosive events lead to a range of immediate atmospheric impacts (Robock, 2000). However, given the infrequency of these very dramatic events and the short lifetime of particles in the atmosphere, a more enduring role (particularly on local scales) is played by the modest but persistent emissions from a large number of quiescently degassing volcanoes, such as Erebus (Antarctica), Etna (Sicily), Villarrica (Chile) and Masaya (Nicaragua). The importance of these aerosol emissions to local tropospheric chemistry is supported by recent studies showing the rapid oxidation of volcanic gases, such as HBr ([Bobrowski et al., 2003] and [Oppenheimer et al., 2006]), HCl ([Bobrowski et al., 2007] and [Kern et al., 2009]), and Hg (von Glasow, 2010), either within or on the surface of volcanic aerosol, and non-magmatic species including NO_y that become involved in volcanic plume chemistry ([Roberts et al., 2009] and [Oppenheimer et al., 2010]). These oxidation processes occur at significantly greater rates than observed in the background atmosphere due to the unique chemistry of quiescent volcanic plumes (e.g., Mather, 2008). Volcanic aerosol may also influence local tropospheric acidity due to the abundance of acidic species (e.g., SO_2, HCl, HF) in volcanic emissions (von Glasow et al., 2009).

The characterisation of quiescent volcanic aerosol has advanced significantly in recent years through the use of cascade impactors (e.g., Hinds, 1999), which aerodynamically size and collect the aerosol for chemical analysis, allowing the determination of composition-resolved size distributions ([Mather et al., 2003], [Mather et al., 2004b], [Martin et al., 2008] and [Ilyinskaya et al., 2010]). Common features of quiescent volcanic aerosol include a concentration of aerosol mass in the 0.1–10 μm size range, high solubility in water, and strong associations between SO_4^{2-}, Na^+ and K^+. However, there is also diversity with some volcanic aerosols dominated by sulphate (e.g., Etna, Villarrica, Masaya, Kilauea) and others by chloride (Erebus), and variations in the number of size modes, their modal diameters and their compositions. Given the mostly secondary nature of volcanic aerosol, these differences may reflect differences in magmatic gas compositions, ambient atmospheric conditions or vent dynamics (e.g., [Martin et al., 2006] and [Branan et al., 2008]). A fundamental uncertainty is whether the reported size distributions from a given volcano are persistent and stable, or whether sampling during short field campaigns offers an unrepresentative snapshot of the volcanic aerosol at each system.

A limitation of cascade impaction is that the technique offers only the mean composition in each size fraction and long sampling durations (>2 h) are often required to collect analysable quantities of aerosol. Increased flow rates with high volume samplers may give insights into how the aerosol evolves with time or with changing ambient conditions, but no information is offered on whether internal or external mixtures are present. Some of these limitations may be addressed by combining results with those from complementary techniques. Optical particle sizing, using either the Sun (i.e., Sun photometry; [Watson and Oppenheimer, 2000] and [Martin et al., 2009]) or an on-board laser (i.e., “dust counters”; [Allen et al., 2006] and [Martin et al., 2009]) as a light source offers time-resolved but not composition-resolved size distributions. Bulk particle sampling, followed by imaging and analysis of filters (e.g., Toutain et al., 1995) offers detailed investigation of single particles (i.e., particles with similar sizes but different compositions can be distinguished) but is not time-resolved. Also, as the number of particles analysed is typically small, it may not be possible to estimate representative size distributions.

2. Masaya volcano

Masaya (elevation ~600 m, 11°59′04″ N, 86°10′06″ W) is a basaltic volcano in Nicaragua that sustains a vigorous and persistent plume from its currently active Santiago crater. Eruptions are rare at Masaya (the most significant event of the last 30 years was a small phreatic explosion in 2001; Duffell et al., 2003), while the quiescent gas and aerosol emissions are amongst the most prodigious of the Central American arc volcanoes (Mather et al., 2006b). Quiescent activity at Masaya has persisted for at least 150 years ([Stoiber et al., 1986] and [Rymer et al., 1998]) and, over the last two decades, the total volatile flux (H_2O, CO_2, SO_2, HCl, HF, etc.) had varied in the range of 10,000–30,000 Mg d^{-1} (Martin et al., 2010). In contrast, there is short-term (i.e., within a field campaign) and long-term (i.e., between field campaigns) stability in the composition of the gas emissions ([Horrocks et al., 1999] and [Martin et al., in press]). The volcanic aerosol from Masaya is arguably the best characterised worldwide. The first use of a cascade impactor for sampling near-source, quiescent volcanic aerosol was made at Masaya in December 2001 (Mather et al., 2003) and showed a fine <1 μm SO_4^{2-}–Na^+–K^+ mode and a coarser >1 μm Cl^-–F^-–Mg^{2+}–Ca^{2+} mode. These results are in agreement with results from size-selective filter sampling at Masaya ([Allen et al., 2002] and [Mather et al., 2006b]). Thermodynamic models (e.g., Symonds and Reed, 1993) predict degassing of metals as chlorides and fluorides (rather than sulphates) so it is expected that the metal halides first condense as salts at high-temperature and subsequently react with H_2SO_4 (formed at low-temperature by the reaction of SO_3 with water, e.g., Mather et al., 2006a) to form metal sulphates and revolatilise HCl and HF. More minor components of the aerosol, including silicates and sulphides (Martin et al., 2009) and trace metals (Moune et al., 2010) have also been characterised using a range of analytical techniques (e.g., energy dispersive x-ray spectroscopy, inductively coupled plasma mass spectrometry). These compositional measurements are supported by optical measurements of the time-resolved size distribution ([Nadeau and Williams-Jones, 2009] and [Martin et al., 2009]).

In this work, we present results from cascade impaction sampling of Masaya's volcanic aerosol during three field campaigns conducted in 2007, 2009 and 2010. Samples were analysed using ion chromatography to determine size distributions in terms of SO_4^{2-}, Cl^-, F^-, NO_3^-, Na^+, K^+, Ca^{2+}, Mg^{2+} and NH_4^+ in the >0.01 μm (aerodynamic) diameter range. A 14-stage nano- Micro Orifice Uniform Deposition Impactor (nano-MOUDI; 0.01–>18 μm) was used in 2007 (n = 10 samples) and 2009 (n = 5 samples) and a 4-stage Sioutas impactor (0.25–>2.5 μm) was used in 2010 (n = 5 samples). Previous studies show compatibility between results from MOUDI and Sioutas impactor ([Misra et al., 2002] and [Singh et al., 2003]) subject to the reduced size range and resolution offered by the Sioutas impactor. The composition-resolved size distributions will be explored with an equilibrium model (ISORROPIA II; Fountoukis and Nenes, 2007) to assess speciation and the overall size distribution (i.e., including condensed water) of the aerosol. The main aims of the study are to (1) assess whether the reported size distributions of volcanic aerosol at Masaya in 2001 (Mather et al., 2003) are stable and persistent, (2) assess the suitability of the Sioutas impactor for volcanic aerosol sampling, and (3) demonstrate the applicability of a thermodynamic model, ISORROPIA II, to investigations of volcanic aerosol. The large number of cascade impaction samples (n = 20 samples) offers one of the most comprehensive investigations of volcanic aerosol to date.

3. Methodology

Fieldwork was conducted in Nicaragua from 8th April to 15th April 2007, 20th March to 24th March 2009, and 29th March to 12th April 2010. The volcanic plume was sampled in all years by cascade impaction (nano-MOUDI in 2007, 2009; Sioutas impactor in 2010; Table 1) from the Sapper Car Park on the SW rim of Santiago crater (Fig. 1). This site is frequently exposed to concentrated emissions as prevailing winds transport the plume to the SW (e.g., in 2010, a personal SO_2 sensor recorded daily means in the 1–5 ppmv range). An additional sample was collected from the Main Car Park in 2007, due to a change in the wind direction that transported the plume to the NW. The age of the plume at the time of sampling was ~1–2 min, estimated by visual tracking of gas puffs. The plume was transparent during the day and more condensed in the evening/night due to increased relative humidity (Mather et al., 2003). Samples were also collected from a range of locations exposed to either no plume (i.e., upwind) or very dilute plume (i.e., >1 km downwind, and in one case in 2009, a sheltered location to the SE of the crater rim). SO_2 fluxes from Masaya were relatively high during the 2007 campaign (~1500 Mg d^{-1}; Kern et al., 2009) and much lower during the 2009 (690 Mg d^{-1}; Martin et al., 2010) and 2010 campaigns (500 Mg d^{-1}; *unpublished data*). There was no explosive activity during any of the three campaigns.

3.1. Direct sampling and analyses

Cascade impactors collect particles through inertial impaction onto a series of stages (see Hinds, 1999 for theoretical details of the technique). The stated cut-off diameters (at 10 L min^{-1}) for impaction on each of the 14 stages of the nano-MOUDI are >18, 10, 5.6, 3.2, 1.8, 1, 0.56, 0.32, 0.18, 0.1, 0.056, 0.032, 0.018, 0.01 μm. The stated cut-off diameters (at 9 L min^{-1}) for the 4 stages of the Sioutas impactor are >2.5, 1, 0.5 and 0.25 μm. The 0.25 μm stage was damaged on an earlier field campaign so was not used in this study. Filter membranes are placed on each stage to collect particles (nanoMOUDI: PTFE, 47 mm, 0.2 μm pore size, Sioutas impactor: laminated PTFE, 25 mm, 0.5 μm pore). In the Sioutas impactor, particles smaller than the lowest cut-off diameter (i.e., <0.25 μm, or <0.5 μm in this case) are collected by filtration (PTFE with PMP support ring, 37 mm, 2.0 μm pore size).

In our hotel room, the impactors were loaded with filters (using nitrile gloves and PTFE tweezers) and wrapped tightly with sealing film. At the sampling site, the nano-MOUDI outlet was connected to a portable Charles Austen Capex V2 DE pump powered by a 12 V car battery. The flow-rate was typically 8–9 L min^{-1} (mean 2007 = 8.8 L min^{-1}; mean 2009 = 8.4 L min^{-1}) and remained stable throughout the sampling duration. Similarly, the Sioutas impactor outlet was connected to a portable Leland Legacy pump powered by an on-board battery. The flow-rate was maintained at 10 L min^{-1} to allow finer discrimination of particle sizes than at 9 L min^{-1}. In 2010, a personal SO_2 sensor (BW Technologies GasAlert Extreme) was used to estimate mean SO_2 concentrations at in-plume sampling sites over the sampling duration. Ambient meteorological conditions (i.e., temperature, relative humidity) were monitored continuously in 2009 and 2010 using a Lascar Electronics datalogger (EL-USB-2-LCD), and non-continuously in 2007 using a portable weather station. In the latter case, the measurement of relative humidity was unstable and few measurements were possible. These meteorological measurements were made from the crater rim but away from the sampling site in relatively clean air. After sampling (>2 h), the pumps were disconnected and the impactor inlets were sealed. Back in the hotel room, the impactors were disassembled and the filters transferred to clean, polypropylene ziploc sample bags. The impactors were then reloaded for the next sample.

In a regular laboratory, the filters were transferred into metal-free polypropylene vials pre-cleaned with the ultra-pure DI water. The hydrophobic PTFE filters were then wet with a few drops of propan-2-ol, and ultra-pure DI water was added to make a solution of 30 ml (2007), 15 ml (2009) or 5 ml (2010). The solutions were placed on a mechanical shaker for at least 30 min to promote extraction. This mild (i.e., at room temperature and neutral pH) procedure extracts mainly the water-soluble fraction of the aerosol. The extracts were analysed undiluted using ion chromatography (Dionex ICS-2000 at University of Birmingham for 2007 samples; Dionex ICS-3000 at University of Cambridge for 2009 and 2010 samples) for anions (SO_4^{2-}, Cl^-, F^-, NO_3^-) and cations (Na^+, K^+, Mg^{2+}, Ca^{2+}, NH_4^+). Samples from 2007 were analysed for anions only. Field blanks of each type of filter (from each campaign) were extracted and analysed similarly to allow for blank correction. For anions, the IC was calibrated using dilutions of single ion standards (SO_4^{2-}, Cl^-, F^-, NO_3^-; Fisher Scientific J/4564/05, J/4546/05, J/4548/05, J/4556/05). For cations, the IC was calibrated using dilutions of a mixed ion standard (Na^+, K^+, Mg^{2+}, Ca^{2+}, NH_4^+; Fisher Scientific J/4554/05). Analysis of the calibration standards indicates typical uncertainties of <5–10% in the determination of extract concentrations.

The concentrations of ions in the extract solutions (in ppm) from each size fraction can be readily converted into a size distribution, $[X]$ (μmol m^{-3}), with the flow-rate, sampling duration, volume of extract solution, and molar mass of each of the ions. This final calculation does not introduce significant additional uncertainties and we estimate an overall uncertainty of <10% on $[X]$.

3.2. Thermodynamic modelling

The thermodynamic Advanced Inorganics Model (AIM; Wexler and Clegg, 2002) has been applied to study volcanic aerosol (e.g., [Mather et al., 2004b], [Oppenheimer et al., 2006], [Martin et al., 2008] and [Roberts et al., 2009]). AIM calculates equilibrium speciation and the amount of water condensed at equilibrium with an aerosol composition at the ambient temperature and relative humidity. Assuming an internal mixture within each size fraction, we may calculate overall size distributions (Mather et al., 2004b).

A limitation of AIM is that it does not consider K^+, Ca^{2+} and Mg^{2+} and the only metal ion specified in the input is Na^+. Measurements at Masaya (Mather et al., 2003) have indicated that the proportions of K^+, Ca^{2+} and Mg^{2+} relative to Na^+ are much higher than in other natural aerosols (e.g., sea-salt aerosols, Heintzenberg et al., 2000). Furthermore, the relative proportions of different metals vary through the size distribution, with coarser particles being richer in Mg^{2+} and Ca^{2+}. Hence Na^+, K^+, Ca^{2+} and Mg^{2+} should be considered separately to model Masaya's aerosol more accurately. A suitable model is ISORROPIA II (Fountoukis and Nenes, 2007), which considers SO_4^{2-}, Cl^-, NO_3^-, H^+, Na^+, K^+, Mg^{2+}, Ca^{2+} and NH_4^+ chemistry. An important difference (Zhang et al., 2000) between the ISORROPIA II model (and its predecessor, ISORROPIA) and AIM is that while the latter is theoretically complete, ISORROPIA II applies several simplifying assumptions to improve computational efficiency (allowing for inclusion within larger models for air quality, e.g., Yu et al., 2005). Despite these simplifying assumptions several studies have shown good agreement between the two models (e.g., [Zhang et al., 2000], [Yu et al., 2005] and [Yao et al., 2006]).

An important issue is whether equilibrium can be assumed between volcanic aerosol in each size fraction and the gas phase, over the short timescales between emission and sampling (~1–2 min). This equilibrium assumption is generally accepted for studies of aerosol in the

background atmosphere; however, such aerosols are undoubtedly older than the aerosol sampled at Masaya. We therefore identify the model results as thermodynamic predictions. Even if equilibrium has not been attained at the crater-rim, equilibrium may be attained further downwind. It is in these older volcanic plumes that rapid heterogeneous oxidation processes are thought to occur (e.g., [Oppenheimer et al., 2006], [Oppenheimer et al., 2010], [Bobrowski et al., 2007], [Roberts et al., 2009] and [von Glasow, 2010]) so our results will have direct bearing on these studies.

4. Results and discussion

4.1. Composition-resolved size distributions from cascade impactor sampling

Previous studies have shown approximately proportional relationships (over a single campaign) between SO_2, SO_4^{2-}, Na^+, K^+, Ca^{2+} and Mg^{2+} concentrations in Masaya's plume ([Allen et al., 2002], [Mather et al., 2006b] and [Martin et al., in press]). Relationships between SO_2 and F^-, Cl^- and NO_3^- are less clear, though, assuming a volcanic origin (e.g., [Mather et al., 2003] and [Mather et al., 2004a]), we would expect increased concentrations of these species in more concentrated plumes (i.e., increased SO_4^{2-}). Therefore, to remove the effects of varying plume dilution, we divide the size distributions for each impactor run, [*X*] (μmol m^{-3}) by $[SO_4^{2-}]_{tot}$ (i.e., the sum of $[SO_4^{2-}]$ over all size fractions) and then average over all in-plume samples for the campaign. This normalised size distribution, mean $([X]/[SO_4^{2-}]_{tot})$, allows the most systematic features of the aerosol to be emphasised, allows for presentation of a large number of samples in a single figure and generates a single aerosol composition for the purposes of modelling.

Normalised size distributions from nano-MOUDI sampling in-plume are shown in Fig. 2 (for SO_4^{2-}, Cl^-, F^-, NO_3^- Na^+, K^+, Ca^{2+} and Mg^{2+}). The cut-off diameters are >19, 11, 6.0, 3.5, 1.9, 1.1, 0.6, 0.35, 0.19, 0.11, 0.06, 0.035, 0.019 μm, based on the mean flow rate, *F*, of 8.6 L min^{-1} and the standard scaling factor of $\sqrt{(F_0/F)}$ (e.g., [Hinds, 1999] and [Mather et al., 2003]) where F_0 = 10 L min^{-1}. Full results are given in Appendix 1. Our findings compare well with earlier results (Mather et al., 2003) showing a fine <1 μm SO_4^{2-}–Na^+–K^+ mode and a coarse >1 μm Cl^-–F^-–Mg^{2+}–Ca^{2+} mode. However, the increased number of samples considered and the enhanced capabilities of the nano-MOUDI allow for more detailed observations. SO_4^{2-} shows modes at <1 μm and >1 μm in 2007 and 2009, despite being uni-modal at <1 μm in 2001. In 2007 the modes occur at 0.35 μm and 1.9 μm, while in 2009 they occur at 0.6 μm and 3.5 μm. In both 2007 and 2009 the <1 μm mode is more abundant than the >1 μm mode so there is an overall consistency with earlier results. The actual increase in modal diameters in 2009 may be smaller or larger than ~2× depending on where the true modal diameters lie relative to the cut-off diameters. The (single) SO_4^{2-} mode in 2001 was centred at ~0.45 μm (Mather et al., 2003), with adjacent stages corresponding to 0.74 μm and 0.24 μm so it is not possible to determine whether the aerosol was more similar to the 2007 or 2009 aerosol. Na^+ and K^+ correspond strongly with SO_4^{2-} in 2009, although the ratio Na^+/K^+ is increased in the coarse SO_4^{2-} mode, and in the largest particles within the fine SO_4^{2-} mode. Ca^{2+} shows a very similar size distribution to Mg^{2+} both having modal diameters at 3.5 μm and >19 μm. The smaller of these modes corresponds with the coarse SO_4^{2-} mode. While Mather et al. (2003) show bimodal Ca^{2+} and Mg^{2+}, the finer of these modes occurs at <1 μm, which was not the case in 2009. Concentrations of Cl^- and F^- were low in 2009 but maxima generally occur at >1 μm and correspond well with maxima in 2007. An additional maxima in Cl^- at 0.11 μm was also observed in three of the four 2009 samples. NO_3^- was below detection limits (~0.0001 μmol m^{-3}) in all but one of the in-plume samples from 2007 and all

of the in-plume samples from 2009. Filter pack measurements from 2009 showed NO_3^-/SO_4^{2-} = 0.02 (Martin et al., 2010) so it is likely that the NO_3^- was distributed across a wide range of particle sizes. NH_4^+ was below detection limits (~0.0001 μmol m^{-3}) in all samples from 2009. This observation indicates that NH_4^+ in Masaya's aerosol (Mather et al., 2003) was formed by neutralisation of NH_3 emissions from some transient or seasonal (i.e., present in December but not March/April) local source, such as agriculture or industry. This observation also supports measurements at Masaya showing that NH_3 is not a volcanic emission (Mather et al., 2003).

A limitation of nano-MOUDI sampling is the significant weight of the impactor (4 kg), along with the required pump (1 kg) and 12 V car battery (~15 kg for 60 A h). In contrast, the Sioutas impactor (160 g) with pump and on-board battery (1 kg) is smaller, lighter and may be run continuously for up to 24 h. Normalised size distributions from Sioutas impactor sampling at Masaya's crater-rim in 2010 are shown in Fig. 3 (for SO_4^{2-}, Cl^-, F^-, Na^+, K^+, Mg^{2+} and Ca^{2+}; NO_3^- and NH_4^+ were always below detection limits of 0.0001 μmol m^{-3}). The cut-off diameters are >2.4, 0.95 and 0.47 μm, for a flow-rate, *F*, of 10 L min^{-1} (e.g., [Hinds, 1999] and [Mather et al., 2003]). Particles < 0.47 μm were collected by filtration and, for plotting, we assume a lower bound of 0.1 μm. The main trends for the 2010 in-plume samples are: (1) SO_4^{2-} modes at <0.47 μm and >2.4 μm, (2) Strong correspondence of Na^+ and K^+ with SO_4^{2-}, with increased Na^+/K^+ ratio in the coarse SO_4^{2-} mode, (3) maxima for F^- or Cl^- at <0.47 μm or >2.4 μm, and (4) maxima for Mg^{2+} at >2.4 μm. Additionally, the only sample from 2010 (10/1) where Ca^{2+} was above detection limits (~0.0001 μmol m^{-3}) was for >2.4 μm.

Previous studies have demonstrated compatibility between results from MOUDI and Sioutas impactor ([Misra et al., 2002] and [Singh et al., 2003]) although it remains to be seen whether the reduced size resolution of the Sioutas impactor poses a serious limitation for the characterisation of quiescent volcanic aerosol. The results from 2007 and 2009 (from nano-MOUDI sampling) were re-binned for compatibility to the size fractions of the Sioutas impactor (>2.4, 0.95, 0.47 and <0.47 μm) and shown in Fig. 3. The features of the size distributions for Cl^-, F^-, Ca^{2+} and Mg^{2+} are mostly retained after re-binning. In contrast, bimodality is no longer shown for SO_4^{2-}, Na^+ and K^+. While the fine and coarse SO_4^{2-} modes (i.e., 0.35 and 1.9 μm in 2007; 0.6 and 3.5 μm in 2009) are placed into non-adjacent size fractions after re-binning (i.e., <0.47 and 0.95 μm in 2007; 0.47 μm and >2.4 μm in 2009), the intermediate nano-MOUDI stages (e.g., 0.6 and 1.1 μm in 2007) are placed into a single size fraction so these no longer appear as minima. This comparison suggests that the Sioutas impactor may be less suitable than nano-MOUDI for the characterisation of closely-spaced modes in volcanic aerosol and for assessing the extreme size limits of fine and coarse modes (e.g., it is not evident in the re-binned results that there is little SO_4^{2-} below 0.1 μm). This poses a significant limitation in terms of assessing important properties of the aerosol, such as atmospheric lifetimes, surface area and the potential to act as cloud condensation nuclei. However, widely-spaced modes are resolvable and associations between ions may still be assessed. Although the nano-MOUDI remains a more optimal instrument for the characterisation of quiescent volcanic aerosol, the Sioutas impactor may be useful at volcanoes where access to near-source emissions is less straightforward than at Masaya.

We now consider the results from 2010 in the context of the earlier results. Since bimodality is shown for SO_4^{2-} in 2010, it seems likely that the two SO_4^{2-} modes were more widely-spaced than in 2007 or 2009, and that the fine SO_4^{2-} mode must have been <0.47 μm (i.e., more similar to 2007 than 2009). The correspondences between Na^+, K^+ and SO_4^{2-}, and between Mg^{2+}, Ca^{2+}, Cl^- and F^-, are shown in 2001, 2009 and 2010, indicating that these are

persistent features of the volcanic aerosol. The variability in abundances between years reflects variability in concentration ratios to SO_4^{2-}. Na^+/SO_4^{2-} and K^+/SO_4^{2-} are somewhat lower in 2010 than in previous campaigns (Table 2). An important contributor to these differences is the increased SO_4^{2-}/SO_2 (Table 2) in 2010. SO_4^{2-} is thought to form by high-T oxidation of SO_2 to SO_3 at the vent by atmospheric oxygen followed by reaction with H_2O (e.g., Mather et al., 2006a) to form H_2SO_4. Increased SO_4^{2-}/SO_2 in 2010 may reflect an increased efficiency of mixing near the vent, allowing for increased oxidation of SO_2. An additional influence on Na^+/SO_4^{2-} and K^+/SO_4^{2-} is variability in the degassing of NaCl and KCl (i.e., the predicted forms of Na and K in high temperature gases; Symonds and Reed, 1993). While size distributions are controlled by a large number of factors, we may exclude the simplest possibility that the change in the modal diameters of SO_4^{2-} – rich modes is due to water uptake from the ambient atmosphere. The relative humidity was especially low in the 2009 (mean 41% RH; Table 1) campaign, while 2010 (mean 46% RH; Table 1), and 2007 (mean >60% RH; Table 1) were generally more humid. Furthermore, from charge balance considerations, we would predict that the aerosol of 2010 would have been more H^+-rich and thus more hygroscopic (e.g., Mather et al., 2004b) than the Na^+, K^+-rich aerosol of 2009.

The bulk aerosol composition, $[X]_{tot}$ (μmol m^{-3}), may be assessed by the summation of results from all stages within a sample. Results are summarised in Fig. 4, as the mean bulk aerosol composition for all in-plume and out-of-plume samples in each year. Different types of out-of-plume samples (e.g., downwind, upwind) are not distinguished in Fig. 4 as they showed similar characteristics. SO_4^{2-}, Na^+, K^+, Mg^{2+} and Ca^{2+} were significantly elevated in-plume in all years, confirming a volcanic origin. It can be further shown that SO_4^{2-}, Na^+, K^+, Mg^{2+} and Ca^{2+} are proportionally related, as found previously (e.g., Martin et al., 2010). In contrast, Cl^- is lower in-plume in all years, while F^- is lower in-plume in 2007 but elevated in-plume in 2009 and 2010. NO_3^- was lower in-plume in 2007 and was below detection limits in impactor samples from 2009 and 2010. However, results from bulk particle filters in 2009 (Martin et al., 2010) show a linear correlation between SO_4^{2-} and NO_3^-.

Our results indicate that Cl^-, and perhaps also F^- and NO_3^-, are displaced from the background aerosol (containing dilute HCl, HF and HNO_3) after mixing with H_2SO_4-rich volcanic aerosol (e.g., Mather et al., 2003). However, other factors must also play a role to explain the in-plume levels of aerosol Cl^-, F^-, and NO_3^- found in this study and/or by Mather et al. (2003). At low RH, the volcanic aerosol would be mostly solid or a highly concentrated acidic solution; either of which would inhibit partitioning of volcanic HCl, HF and HNO_3 gas into the aerosol. At high RH, the volcanic aerosol would take up water to form a less acidic solution, enabling uptake of volcanic HCl, HF and HNO_3 (to varying extents). Furthermore, as the volume of the volcanic aerosol increases (due to hygroscopic growth), uptake would be further promoted by Henry's Law. This interpretation may explain why an in-plume elevation of Cl^- was found by Mather et al. (2003), who sampled in December 2001 in cooler, more humid conditions (mean 81% RH, 25 °C) than in the present study, where samples were typically collected in hotter, drier conditions in March/April. This apparent depletion of Cl^- from Masaya's aerosol has important implications for the formation of ClO and OClO. A recent study using active differential optical absorption spectroscopy (DOAS) (Kern et al., 2009) did not detect either ClO or OClO in Masaya's plume in mid April 2007 (the week following our 2007 campaign). While there are methodological reasons (Kern et al., 2009) to suggest that earlier studies may have overestimated ClO emissions at Masaya and elsewhere (e.g., [Lee et al., 2005] and [Bobrowski et al., 2007]), our results suggest that ClO and OClO formation at Masaya in April 2007 could have been hindered by depletion of Cl^- from the volcanic aerosol at source. While it may be expected that Masaya's aerosol would also be depleted in Br^- (HBr is a strong acid, like HCl), BrO was detected by Kern et al. (2009). It may be that BrO production is less sensitive to the initial composition of the

aerosol, since the uptake of additional HBr is much faster than the uptake of additional HCl (due to the increased acidity constant of HBr; Bobrowski et al., 2007).

4.2. Thermodynamic modelling

Input compositions (Table 3) for ISORROPIA II were generated by multiplying the normalised size distributions, mean ($[X]/[SO_4^{2-}]_{tot}$), in 2009 and 2010 by mean $[SO_4^{2-}]_{tot}$ over all in-plume samples (3 μmol m^{-3}). Model calculations were made for speciation over the range 10% < RH < 95% at 35 °C (the model results are not highly sensitive to temperature). The 2007 aerosol composition was not modelled because only anions were analysed. Excess negative charge is assumed to be balanced by H^+. We cannot exclude the possibility that some of this excess negative charge is balanced by unmeasured metal cations such as Al^{3+} and Pb^{2+} (e.g., Ilyinskaya et al., 2010) and acknowledge that this is a limitation of the study. H^+/SO_4^{2-} was estimated to be 0.9 in 2009 (Martin et al., in press) and 1.6 in 2010. In general, increased H^+/SO_4^{2-} corresponds to increased hygroscopicity (e.g., Mather et al., 2004b). Excess positive charge was balanced by X^-, and Cl^-, F^- and X^- were entered together as Cl^-. To improve numerical stability, no more than four decimal places were used for inputs and any zero quantities were input as 0.0001 μmol m^{-3}. The model was run as a "reverse problem" where concentrations of $HCl_{(g)}$, $HNO_{3(g)}$ and $NH_{3(g)}$ are calculated from the input aerosol composition.

Fig. 5 shows model results for equilibrium speciation in the fine SO_4^{2-}-rich modes in 2009 (0.6 μm) and 2010 (<0.47 μm), and the coarse SO_4^{2-}-rich modes in 2009 (3.5 μm) and 2010 (>2.4 μm). $NaHSO_4$, $KHSO_4$, $CaSO_4$ and $MgSO_4$ are the major forms of the ions in the dry aerosol in both SO_4^{2-}-rich modes in 2009. The coarse SO_4^{2-}-rich mode also shows some Na_2SO_4. Na^+, K^+, H^+, Mg^{2+}, HSO_4^-, SO_4^{2-}, and $CaSO_4$ are the major forms in the wet aerosol in both SO_4^{2-}-rich modes in 2009. The insolubility of $CaSO_4$ is assumed by the ISORROPIA II model. $NaHSO_4$ is more sensitive to increasing RH than $KHSO_4$, so increased Na^+/K^+ in the coarse SO_4^{2-}-rich mode allows deliquescence at lower RH (~40% RH) than in the fine SO_4^{2-}-rich mode (~50% RH). In 2010, H^+, HSO_4^-, $NaHSO_4$, $KHSO_4$ and Mg^{2+} are the major forms in both SO_4^{2-}-rich modes at 10% RH. However, the hygroscopic nature of the aerosol (i.e., high H^+/SO_4^{2-}) hastens the dissolution of $NaHSO_4$ and $KHSO_4$, and Na^+ and K^+ are major forms by 20–30% RH. Calculations for equilibrium speciation were also made in the coarse Cl^--rich mode (>19 μm) in 2009. Unfortunately, the calculations were not successful in the dry aerosol (with a poor fit between the input and output totals for each ion) although the major species were predicted to be $CaSO_4$, NaCl and $MgCl_2$. The model was more successful in the wet aerosol (>40% RH), predicting that the major forms were Na^+, K^+, Mg^{2+}, Cl^- and $CaSO_4$. For both 2009 and 2010, there was little agreement between the calculated concentrations of $HCl_{(g)}$ from different stages of the same impactor run. This result suggests an external mixture of acidic Cl^--poor particles (i.e., volcanic aerosol) and less acidic Cl-rich particles (i.e., background aerosol).

Fig. 6 shows model results for total aerosol mass in each size fraction (μg m^{-3}). In 2009, the 0.35–1.1 μm size fractions (i.e., the fine SO_4^{2-}-rich mode) deliquesce close to 50% RH, while the 1.9–3.5 μm size fractions (i.e., the coarse SO_4^{2-}-rich mode) deliquesce closer to 40% RH. Above 50% RH, water uptake is fairly comparable between the two SO_4^{2-}-rich modes. Water uptake occurs at lower RH in the 0.19 μm and 6.0 μm size fractions due to the higher inferred concentrations of H^+. The results for the 11 μm and >19 μm fractions are less straightforward and the model shows instability with water uptake erroneously decreasing at increased RH at times. In the more hygroscopic 2010 aerosol, all size fractions show water uptake at low RH. Based on the typical day-time 30–40% RH,

these results suggest that while the 2009 aerosol was mostly dry (i.e., a salt), the 2010 aerosol was up to 50% (by mass) water (i.e., a solution).

4.3. The potential effects of plume dilution

We have so far assumed that the relative humidity in the plume equals the ambient relative humidity (i.e., measured from the crater rim but away from the sampling site in relatively clean air). This assumption requires that the contribution of magmatic $H_2O_{(g)}$ to total $H_2O_{(g)}$ is negligible. The concentration of ambient $H_2O_{(g)}$ at 1 atm, 35 °C and 40% RH is 2200 ppmv. Based on the maximum SO_2 concentration at the crater-rim in 2010 (35 ppmv), and measurements in 2009 of Masaya's gas composition ($H_2O_{(g)}/SO_2$ = 63, $H_2O_{(g)}$ ~ 90 mol%; Martin et al., 2010), we predict a maximum concentration of magmatic $H_2O_{(g)}$ of 2200 ppmv. The ambient and magmatic contributions are approximately additive because the mixing ratio of magmatic gas is small (~3%), so does not significantly dilute ambient $H_2O_{(g)}$. This analysis indicates that RH in the plume may be greater than ambient RH. Based on the results from thermodynamic modelling, we propose that solid particles would initially undergo water uptake (as the plume cools below the temperature at which salt solutions become stable, i.e., ~100 °C) followed by subsequent water loss as the magmatic $H_2O_{(g)}$ becomes diluted (provided that the timescales of equilibration are sufficiently short). The model results shown in Fig. 5 and Fig. 6 therefore give some indication of how the aerosol may evolve in response to dilution, both before and beyond the crater rim.

A potential explanation for the increased modal diameters in 2009 may be that more concentrated emissions were sampled in 2009 than in other years. This possibility is supported by higher mean SO_2 at the crater-rim in 2009 (~10 ppmv; Martin et al., 2010) compared to in 2010 (~2 ppmv SO_2). In 2009, we predict a mean magmatic $H_2O_{(g)}$ of 630 ppmv, increasing the relative humidity from 40% RH (i.e., ambient) to ~50% RH. Our model calculations suggest the total aerosol mass would increase by only ~20% due to this effect, giving a much smaller (i.e., mass$\propto d^3$) change in particle diameter. Therefore plume dilution cannot explain differences in modal diameters between 2009 and 2010. Furthermore, while no SO_2 measurements were made in 2007, SO_4^{2-} measurements (Fig. 4) indicate that the emissions were the most concentrated of the three campaigns.

5. Conclusions

Volcanic aerosol has now been characterised at a number of volcanoes using cascade impactors. However, a fundamental uncertainty is whether the reported size distributions are persistent and stable, or only a potentially unrepresentative snapshot of the volcanic aerosol at each system.

Masaya volcano (Nicaragua) was the focus of the first impactor study of near-source, quiescent volcanic aerosol in 2001 (Mather et al., 2003). To allow for re-assessment, further impactor samples were collected at Masaya in 2007 and 2009 (using a 14-stage nano-MOUDI) and 2010 (using a 4-stage Sioutas impactor), and analysed using ion chromatography. We found several differences in the volcanic aerosol between the four campaigns: (1) SO_4^{2-} showed modes in both the fine (<1 μm; with low Na^+/K^+) and coarse (>1 μm; with high Na^+/K^+) fractions in all of the recent campaigns despite being unimodal in 2001 (<1 μm); (2) The modal diameters for SO_4^{2-} increased by a factor of ~2× in 2009, compared to 2007 or 2010; (3) total Cl^- was depleted in volcanic aerosol in all the more recent campaigns but was enriched in 2001. Other aspects of the volcanic aerosol are more

persistent, such as the fine SO_4^{2-}–H^+–Na^+–K^+ mode, which was the most abundant mode in all campaigns, along with a coarser Cl^-–F^-–Mg^{2+}–Ca^{2+} mode of lower abundance. These observations are set against a near-constant magmatic gas composition (Martin et al., 2010). The equilibrium model, ISORROPIA II, was used to investigate equilibrium speciation within the volcanic aerosol in 2009 and 2010. Model results show that the coarse SO_4^{2-}-rich mode deliquesces at lower relative humidity (40% RH) than the fine SO_4^{2-}-rich mode (50% RH) due to increased Na^+/K^+ in the former. At ambient relative humidity (~40% RH), the 2009 aerosol was predicted to be dry, while the 2010 aerosol was entirely liquid. This difference is due to proportionally lower concentrations of metals in 2010, consistent with the aerosol being richer in the more hygroscopic H_2SO_4 (i.e., high H^+/SO_4^{2-}) These results indicate that aerosol emissions from a single volcano vary in terms of ionic composition and even more so in terms of physical speciation. We propose that if the origin of these differences at Masaya could be understood, we may better appreciate the atmospheric and dynamic factors that influence the formation of volcanic aerosols elsewhere, since the magmatic gas composition at Masaya is not strongly variable.

Acknowledgements

The work was supported by NERC grants: NE/F004222/1 and NE/F005342/1. We thank the staff of the Parque Nacional Volcan Masaya and INETER for their support, and GG Salerno, L Spampinato, C Ramirez, H Thomas, TJ Roberts and IM Watson for assistance in the field. A Allen is thanked for IC analyses of 2007 samples. RSM acknowledges travel funding from the Percy Sladen Memorial Fund ("Bio-availability of nitrogen deposition around an active volcano").

References

Allen et al., 2002 A.G. Allen, C. Oppenheimer, M. Ferm, P.J. Baxter, L.A. Horrocks, B. Galle, A.J.S. McGonigle, H.J. Duffell Primary sulfate aerosol and associated emissions from Masaya Volcano, Nicaragua Journal of Geophysical Research, 107 (2002), p. 4682

Allen et al., 2006 A.G. Allen, T.A. Mather, A.J.S. McGonigle, A. Aiuppa, P. Delmelle, B. Davison, N. Bobrowski, C. Oppenheimer, D.M. Pyle, S. Inguaggiato Sources, size distribution and downwind grounding of aerosols from Mt. Etna Journal of Geophysical Research, 111 (2006), p. D10302

Bobrowski et al., 2003 N. Bobrowski, G. Honninger, B. Galle, U. Platt Detection of bromine monoxide in a volcanic plume Nature, 423 (2003), pp. 273–276

Bobrowski et al., 2007 N. Bobrowski, R. von Glasow, A. Aiuppa, S. Inguaggiato, I. Louban, O.W. Ibrahim, U. Platt Reactive halogen chemistry in volcanic plumes Journal of Geophysical Research, 112 (2007), p. D06311

Branan et al., 2008 Y. Branan, A. Harris, I.M. Watson, J.C. Phillips, K. Horton, G. Williams-Jones, H. Garbeil Investigation of at-vent dynamics and dilution using thermal infrared radiometers at Masaya volcano, Nicaragua Journal of Volcanology and Geothermal Research, 169 (2008), pp. 34–47

Duffell et al., 2003 H.J. Duffell, C. Oppenheimer, D.M. Pyle, B. Galle, A.J.S. McGonigle, M.R. Burton Changes in gas composition prior to a minor explosive eruption at Masaya

volcano, Nicaragua Journal of Volcanology and Geothermal Research, 126 (2003), pp. 327–339

Fountoukis and Nenes, 2007 C. Fountoukis, A. Nenes ISORROPIA II: a computationally efficient aerosol thermodynamic equilibrium model for K^+, Ca^{2+}, Mg^{2+}, NH_4^+, Na^+, SO_4^{2-}, NO_3^-, Cl^-, H_2O Aerosols Atmospheric Chemistry and Physics, 7 (2007), pp. 4639–4659

Graf et al., 1997 H.F. Graf, J. Feichter, B. Langmann Volcanic degassing: Contribution to global sulphate burden and climate Journal of Geophysical Research, 102 (1997), pp. 107227–110738

Heintzenberg et al., 2000 J. Heintzenberg, D.C. Covert, R. Van Dingenen Size distributions and chemical composition of marine aerosols: a compilation and review Tellus, 52B (2000), pp. 1104–1122

Hinds, 1999 W.C. Hinds Aerosol Technology: Properties, Behavior and Measurement of Aerosol Particles (second ed.)Wiley Interscience (1999) 483 pp

Horrocks et al., 1999 L. Horrocks, M. Burton, P. Francis, C. Oppenheimer Stable gas plume composition measured by OP-FTIR spectroscopy at Masaya Volcano, Nicaragua, 1998–1999 Geophysical Research Letters, 26 (1999), pp. 3497–3500

Ilyinskaya et al., 2010 E. Ilyinskaya, C. Oppenheimer, T.A. Mather, R.S. Martin, P.R. Kyle Chemistry and size distribution of water-soluble aerosol in the plume of Mt Erebus volcano, Antarctica Geochemistry Geophysics Geosystems, 11 (2010), p. Q03017

Kern et al., 2009 C. Kern, H. Sihler, L. Vogel, C. Rivera, M. Herrera, U. Platt Halogen oxide measurements at Masaya Volcano, Nicaragua using active long path differential optical absorption spectroscopy Bulletin of Volcanology, 71 (2009), pp. 659–670

Lee et al., 2005 C. Lee, Y.J. Kim, H. Tanimoto, N. Bobrowski, U. Platt, T. Mori, K. Yamamoto, C.S. Hong High ClO and ozone depletion observed in the plume of Sakurajima volcano, Japan Geophysical Research Letters, 32 (2005), p. L21809

Martin et al., 2006 R.S. Martin, T.A. Mather, D.M. Pyle High-temperature mixtures of magmatic and atmospheric gases Geochemistry Geophysics Geosystems, 7 (2006), p. Q04006

Martin et al., 2008 R.S. Martin, T.A. Mather, D.M. Pyle, M. Power, A.G. Allen, A. Aiuppa, C.J. Horwell, E.P.W. Ward Composition-resolved size distributions of volcanic aerosols in the Mt. Etna plumes Journal of Geophysical Research, 113 (2008), p. D17211

Martin et al., 2009 R.S. Martin, T.A. Mather, D.M. Pyle, M. Power, V.I. Tsanev, C. Oppenheimer, A.G. Allen, C.J. Horwell, E.P.W. Ward Size distributions of fine silicate and other particles in Masaya's volcanic plume Journal of Geophysical Research, 114 (2009), p. D09217

Martin et al., in press Martin, R.S., Sawyer, G.M., Spampinato, L., Salerno, G.G., Ramirez, C., Ilyinskaya, I., Witt, M.L.I., Mather, T.A., Watson, I.M., Phillips, J.C., Oppenheimer, C., 2010. A total volatile inventory for Masaya volcano, Nicaragua. Journal of Geophysical Research, 115, B09215.

Mather et al., 2003 T.A. Mather, A.G. Allen, C. Oppenheimer, D.M. Pyle, A.J.S. McGonigle Size-resolved characterisation of soluble ions in the particles in the tropospheric plume of Masaya volcano, Nicaragua: origins and plume processing Journal of Atmospheric Chemistry, 46 (2003), pp. 207–237

Mather et al., 2004a T.A. Mather, A.G. Allen, B.M. Davison, D.M. Pyle, C. Oppenheimer, A.J.S. McGonigle Nitric acid from Volcanoes Earth and Planetary Science Letters, 218 (2004), pp. 17–30

Mather et al., 2004b T.A. Mather, V.I. Tsanev, D.M. Pyle, A.J.S. McGonigle, C. Oppenheimer, A.G. Allen Characterization and evolution of tropospheric plumes from Lascar and Villarrica volcanoes, Chile Journal of Geophysical Research, 109 (2004), p. D21303

Mather et al., 2006a T.A. Mather, J.R. McCabe, V.K. Rai, M.H. Thiemens, D.M. Pyle, T.H.E. Heaton, H.J. Sloane, G. Fern The oxygen and sulfur isotopic composition of volcanic sulfate aerosol at the point of emission Journal of Geophysical Research, 111 (2006), p. D18205

Mather et al., 2006b T.A. Mather, D.M. Pyle, V.I. Tsanev, A.J.S. McGonigle, C. Oppenheimer, A.G. Allen A reassessment of current volcanic emissions from the Central American arc with specific examples from Nicaragua Journal of Volcanology and Geothermal Research, 149 (2006), pp. 297–311

Mather, 2008 T.A. Mather Volcanoes and the atmosphere: the potential role of the atmosphere in unlocking the reactivity of volcanic emissions Philosophical Transactions A, 366 (2008), pp. 4581–4595

Misra et al., 2002 C. Misra, M. Singh, S. Shen, C. Sioutas, P.M. Hall Development and evaluation of a personal cascade impactor sample (PCIS) Journal of Aerosol Science, 33 (2002), pp. 1027–1047

Moune et al., 2010 S. Moune, P.-J. Gauthier, P. Delmelle Trace elements in the particulate phase of the plume of Masaya Volcano, Nicaragua Journal of Volcanology and Geothermal Research, 193 (2010), pp. 232–244

Nadeau and Williams-Jones, 2009 P.A. Nadeau, G. Williams-Jones Apparent downwind depletion of volcanic SO_2: lessons from Masaya volcano, Nicaragua Bulletin of Volcanology, 71 (2009), pp. 389–400

Oppenheimer et al., 2006 C. Oppenheimer, V.I. Tsanev, C.F. Braban, R.A. Cox, J.W. Adams, A. Aiuppa, N. Bobrowski, P. Delmelle, J. Barclay, A.J.S. McGonigle BrO formation in volcanic plumes Geochimica et Cosmochimica Acta, 70 (2006), pp. 2935–2941

Oppenheimer et al., 2010 C. Oppenheimer, P. Kyle, F. Eisele, J. Crawford, G. Huey, D. Tanner, K. Saewung, L. Mauldin, D. Blake, A. Beyersdorf, M. Buhr, D. Davis Atmospheric chemistry of an Antarctic volcanic plume Journal of Geophysical Research, 115 (2010), p. D04303

Roberts et al., 2009 T.J. Roberts, C.F. Braban, R.S. Martin, C. Oppenheimer, J.W. Adams, R.A. Cox, R.L. Jones, P.T. Griffiths Modelling reactive halogen formation and ozone depletion in volcanic plumes Chemical Geology, 263 (2009), pp. 110–121

Robock, 2000 A. Robock Volcanic eruptions and climate Reviews in Geophysics, 38 (2000), pp. 191–219

Rymer et al., 1998 H. Rymer, B.V. de Vries, J. Stix, G. Williams-Jones Pit crater structure and processes governing persistent activity at Masaya Volcano, Nicaragua Bulletin of Volcanology, 59 (1998), pp. 345–355

Singh et al., 2003 M. Singh, C. Misra, C. Sioutas Field evaluation of a personal cascade impactor sampler (PCIS) Atmospheric Environment, 37 (2003), pp. 4781–4793

Stoiber et al., 1986 R.E. Stoiber, S.N. Williams, B.J. Huebert Sulfur and halogen gases at Masaya caldera complex, Nicaragua – total flux and variations with time Journal of Geophysical Research, 91 (1986), pp. 2215–2231

Symonds and Reed, 1993 R.B. Symonds, M.H. Reed Calculation of multicomponent chemical-equilibria in gas-solid-liquid systems: calculation methods, thermochemical data, and applications to studies of high temperature volcanic gases with examples from Mount St. Helens American Journal Science, 293 (1993), pp. 758–864

Toutain et al., 1995 J.P. Toutain, J.P. Quisefit, P. Briole, P. Aloupogiannis, P. Blanc, G. Robaye Mineralogy and chemistry of solid aerosols emitted from Mount Etna Geochemical Journal, 29 (1995), pp. 163–173

von Glasow, 2010 R. von Glasow Atmospheric chemistry in volcanic plumes Proceedings of the National Academy of Sciences of the Unites States of America, 107 (2010), pp. 6594–6599

von Glasow et al., 2009 R. von Glasow, N. Bobrowksi, C. Kern The effects of volcanic eruptions on atmospheric chemistry Chemical Geology, 263 (2009), pp. 131–142

Watson and Oppenheimer, 2000 I.M. Watson, C. Oppenheimer Particle size distributions of Mt. Etna's aerosol plume constrained by sun-photometry Journal of Geophysical Research, 105 (2000), pp. 9823–9830

Wexler and Clegg, 2002 A.S. Wexler, S.L. Clegg Atmospheric aerosol models for systems including the ions H^+, NH_4^+, Na^+, SO_4^{2-}, NO_3^-, Cl^-, Br^-, and H_2O Journal of Geophysical Research, 107 (2002), p. 4207

Yao et al., 2006 X. Yao, T.Y. Ling, M. Fang, C.K. Chan Comparison of thermodynamic predictions for in situ pH in $PM_{2.5}$ Atmospheric Environment, 40 (2006), pp. 2835–2844

Yu et al., 2005 S. Yu, R. Dennis, S. Roselle, A. Nenes, J.T. Walker, B. Eder, K. Schere, J. Swall, W. Robarge An assessment of the ability of 3-D air quality models with current thermodynamic equilibrium models to predict aerosol NO_3^- Journal of Geophysical Research, 110 (2005), p. D07S13

Figures and Tables

Table 1. Sampling details for 2007, 2009 and 2010 campaigns. The type of sample is denoted IP (in-plume) or OP (out-of-plume). RH is relative humidity, expressed as a percent. Mean SO_2 concentrations at the crater rim (from a personal SO_2 sensor) are given for 2010 samples.

Sample	Type	Location	Date	Time (local)	Flow (L min^{-1})	Duration (min)	Notes[a]
7/1	IP	Sapper Car Park	08/04/2007	0950–1605	9	375	32 °C, >60% RH, few clouds
7/2	IP	Sapper Car Park	09/04/2007	0940–1540	9	360	30 °C, >60% RH, few clouds
7/3	OP	2 km downwind	10/04/2007	1025–1600	9	335	35 °C, >60% RH, mostly cloudy
7/4	IP	Sapper Car Park	11/04/2007	1040–1640	9	300[b]	28 °C, >60% RH, overcast
7/5	IP	Sapper Car Park	12/04/2007	0950–1450	8.5	300	30 °C, >60% RH, mostly cloudy
7/6	IP	Main Car Park	12/04/2007	1700–1945	8.5	165	22 °C, >60% RH, overcast with rain
7/7	IP	Sapper Car Park	13/04/2007	1020–1655	8	395	30 °C, >60% RH, mostly cloudy
7/8	OP	2 km downwind	14/04/2007	0950–1550	8.5	360	32 °C, 71% RH, mostly cloudy
7/9	OP	4 km upwind	14/04/2007	1915–2225	9.5	200	25 °C, >60% RH, mostly cloudy
7/10	OP	3 km upwind	15/04/2007	0850–1620	9	450	35 °C, 68% RH, mostly cloudy
9/1	IP	Sapper Car Park	20/03/2009	0900–1250	8	230	35–38 °C, 30–40% RH, clear
9/2	IP	Sapper Car Park	21/03/2009	0900–1310	9	250	34–39 °C, 32–44% RH, clear
9/3	IP	Sapper Car Park	22/03/2009	0900–1240	8	220	31–37 °C, 32–40% RH, clear
9/4	IP	Sapper Car Park	23/03/2009	0900–1220	9	200	30–35 °C, 37–50% RH, clear
9/5	OP	~100 m upwind	24/03/2009	0900–1210	8	190	25–39 °C, 46–60% RH, mostly cloudy
10/1	IP	Sapper Car Park	07/04/2010	0930–1700	10	450	33–37 °C, 43–57% RH, few clouds, $[SO_2]$ = 0.6 ppm
10/2	IP	Sapper Car Park	08/04/2010	1100–1700	10	360	35–38 °C, 42–43% RH, few clouds, $[SO_2]$ = 1.1 ppm
10/3	IP	Sapper Car Park	09/04/2010	0930–1700	10	450	31–40 °C, 32–42% RH, overcast, $[SO_2]$ = 2.7 ppm
10/4	OP	5 km downwind	10/04/2010	0800–1000	10	120	32–40 °C, 34–40% RH, mostly cloudy
10/5	IP	Sapper Car Park	11/04/2010	1230–1800	10	330	24–36 °C, 56–80% RH, few clouds, $[SO_2]$ = 5.4 ppm

A The RH sensor in 2007 was unstable so only a few measurements could be made. Based on our personal observations of the meteorological conditions, the available RH measurements from our campaign, and the RH measurements made by Kern et al. (2009) in the week following our campaign,

we estimate a mean RH of >60% for all measurement periods where no RH measurements were available.
B The pump was stopped between 1240–1340 for sample 7/4, so the sampling duration was reduced to 300 min.

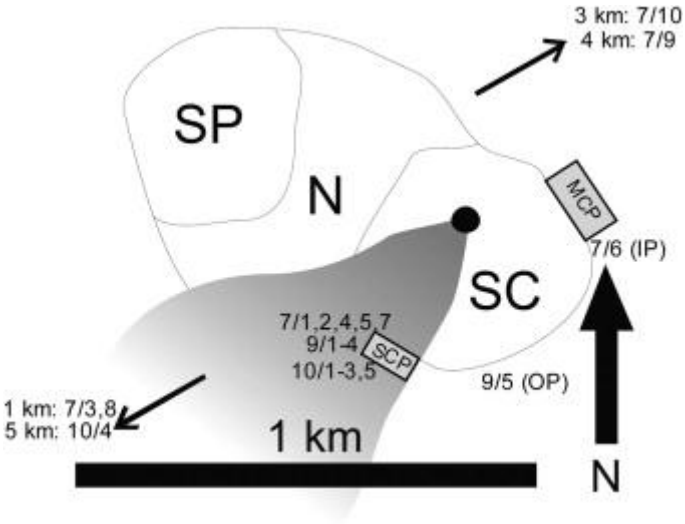

Fig. 1. Map of the summit of Masaya volcano (Nicaragua). The nested craters of Santiago (SC), Nindiri (N) and San Pedro (SP) are shown. The active degassing vent is found at the base of Santiago crater. In-plume sampling was performed from the Sapper Car Park (SCP) on the South-West rim. Other samples collected from around the crater rim were 7/6 (an in-plume sample from the Main Car Park, MCP) and 9/5 (an out-of-plume sample from a sheltered location). The direction and location of other out-of-plume samples are indicated. The most typical direction and width of the plume is indicated by the shaded sector.

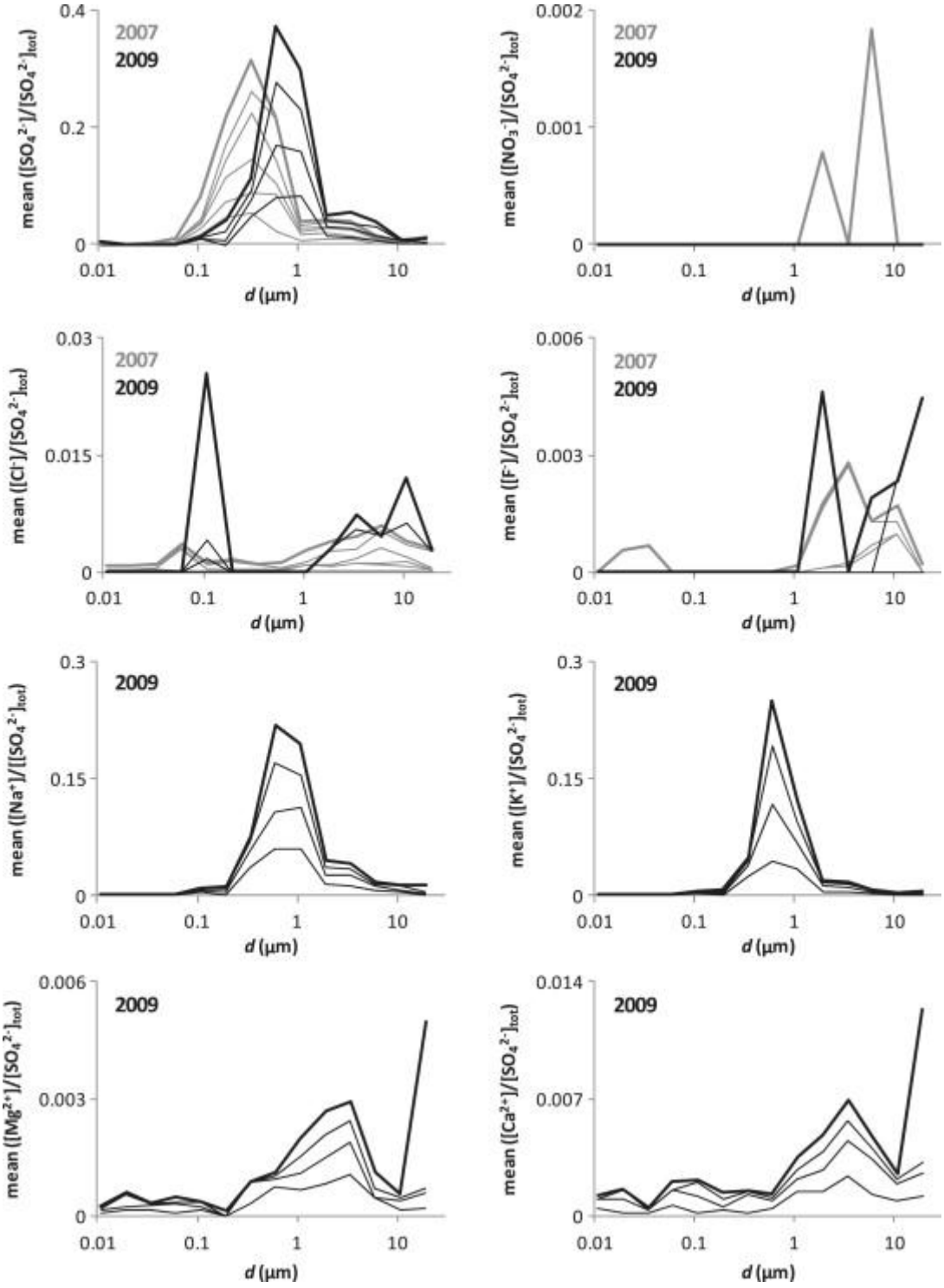

Fig. 2. Normalised size distributions, mean ($[X]/[SO_4^{2-}]_{tot}$), for Masaya's volcanic aerosol in 2007 (dark grey) and 2009 (black). The contributions of individual in-plume samples (with non-zero concentrations) are indicated. Full results are given in Appendix 1. The uncertainties on the vertical axis are <10%.

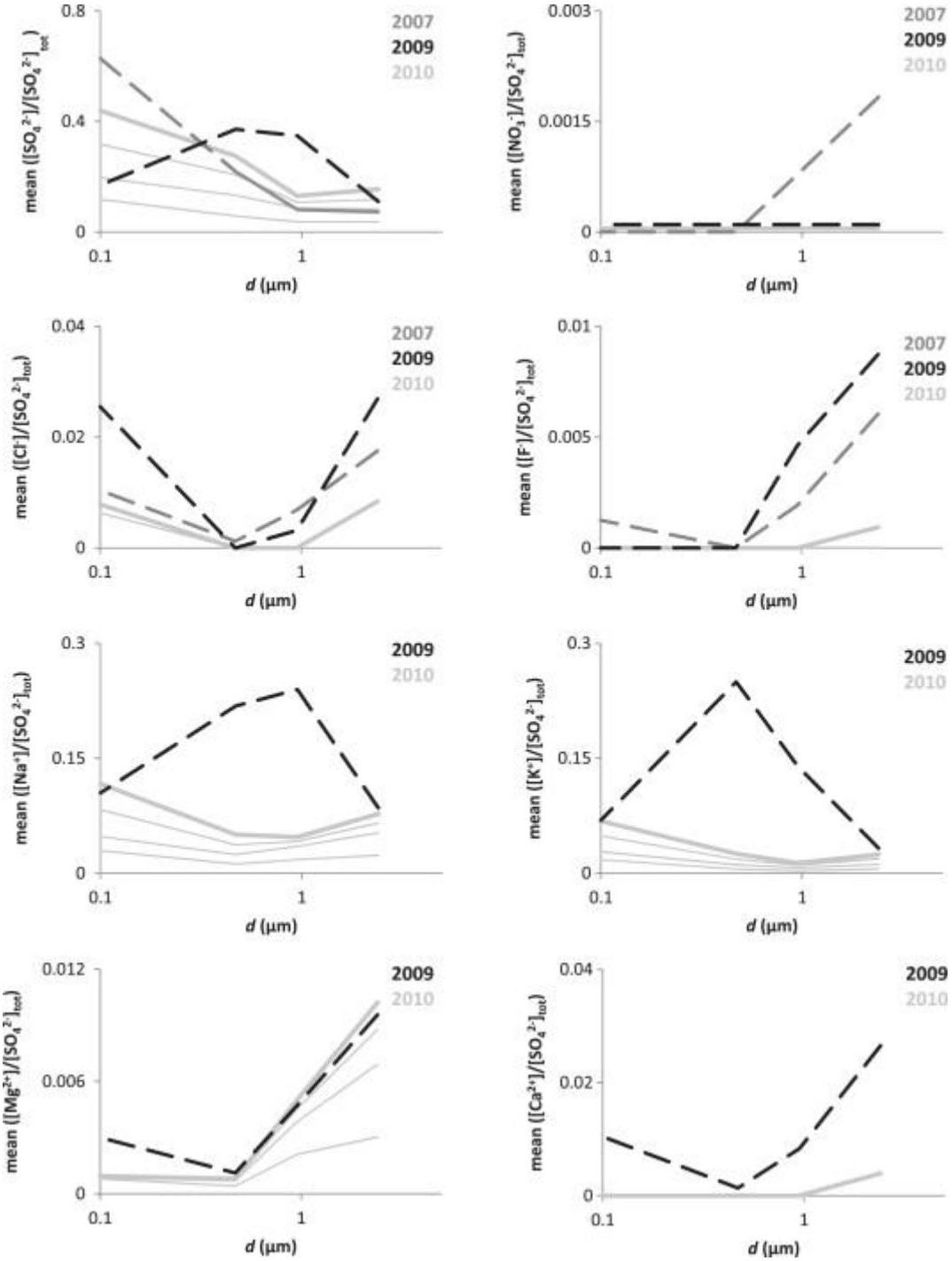

Fig. 3. Normalised size distributions, mean ($[X]/[SO_4^{2-}]_{tot}$), for Masaya's volcanic aerosol in 2010 (light grey). The contributions of individual in-plume samples (with non-zero concentrations) are indicated for 2010. Results from 2007 (dark grey dashed) and 2009 (black dashed) are re-binned for compatibility with Sioutas impactor results. The uncertainties on the vertical axis are <10%.

Table 2. Molar ratios between Na^+, K^+, SO_4^{2-} and SO_2 in Masaya's emissions in 2001, 2003, 2009 and 2010.

	2001[a]	**2003[a]**	**2009[b]**	**2010[c]**
Na^+/SO_4^{2}	1.1	0.70	0.68	0.29
K^+/SO_4^{2-}	0.35	0.49	0.71	0.13
SO_4^{2-}/SO_2	0.013	0.007	0.005	0.020

A : Ratios are means from filter pack measurements (Mather et al., 2003).
B : Ratios are regression gradients from filter pack measurements (Martin et al., in press).
C : Ratios are means from summing Sioutas impactor stages and dividing by $[SO_2]$ (from a personal SO_2 sensor; Table 1).

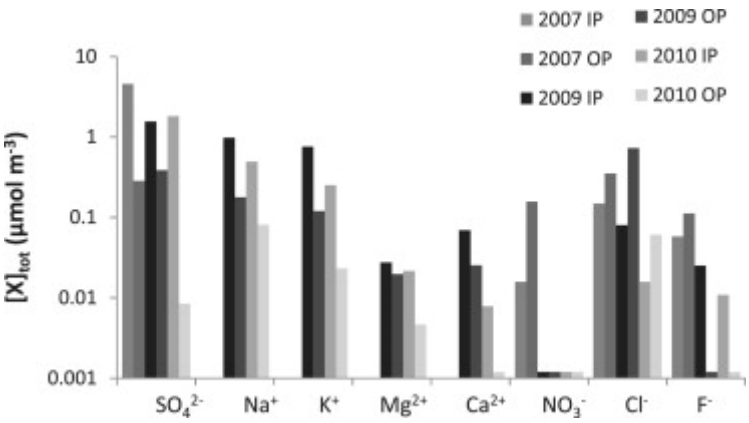

Fig. 4. Bulk aerosol compositions, $[X]_{tot}$ (µmol m^{-3}), for in-plume (IP) and out-of-plume (OP) impactor samples in 2007, 2009 and 2010. Individual results are given in Appendix 1.

Table 3. Model inputs for ISORROPIA II, from the normalised size distributions in 2009 and 2010. Concentrations of ions are given in μmol m^{-3}. Excess charge was balanced by H^+ or X^-. To improve numerical stability, no more than four decimal places were used for inputs and any zero quantities were input as 0.0001 μmol m^{-3}.

Year	*d*/um	SO_4^{2-}	Cl^-	NO_3^-	Na^+	K^+	Mg^{2+}	Ca^{2+}	NH_4^+
2009	>19	0.033	0.090	0.0001	0.039	0.015	0.015	0.036	0.0001
	11	0.019	0.042	0.0001	0.042	0.011	0.0017	0.0075	0.0001
	6	0.12	0.019	0.0001	0.052	0.021	0.0032	0.014	0.0001
	3.5	0.16	0.022	0.0001	0.12	0.049	0.0086	0.020	0.0001
	1.9	0.15	0.023	0.0001	0.13	0.06	0.0080	0.014	0.0001
	1.1	0.90	0.0001	0.0001	0.58	0.35	0.0059	0.010	0.0001
	0.6	1.1	0.0001	0.0001	0.64	0.74	0.0033	0.0040	0.0001
	0.35	0.34	0.0001	0.0001	0.22	0.14	0.0025	0.0044	0.0001
	0.19	0.13	0.0001	0.0001	0.033	0.021	0.0004	0.0041	0.0001
	0.11	0.039	0.075	0.0001	0.028	0.017	0.0011	0.0063	0.0001
	0.06	0.0001	0.036	0.0001	0.0060	0.0075	0.0014	0.0060	0.0001
	0.035	0.0001	0.020	0.0001	0.0063	0.0052	0.0010	0.0016	0.0001
	0.019	0.0001	0.029	0.0001	0.0070	0.0054	0.0018	0.0048	0.0001
	0.011	0.015	0.0001	0.0001	0.0047	0.0043	0.0007	0.0036	0.0001
2010	2.4	0.47	0.028	0.0001	0.23	0.073	0.031	0.012	0.0001
	0.95	0.39	0.0001	0.0001	0.14	0.040	0.015	0.0001	0.0001
	0.47	0.83	0.0001	0.0001	0.15	0.076	0.0024	0.0001	0.0001
	<0.47	1.3	0.023	0.0001	0.35	0.20	0.0028	0.0001	0.0001

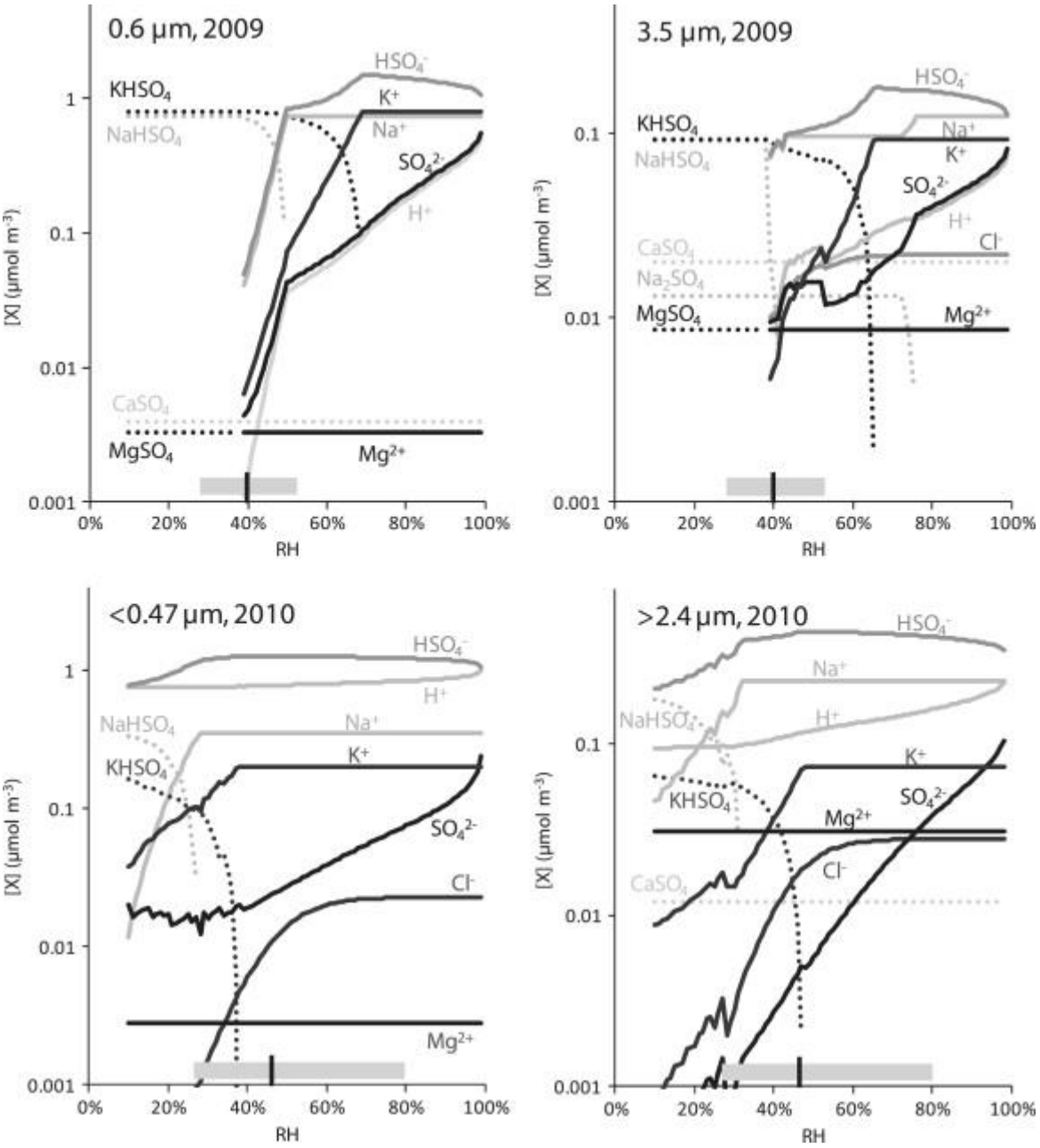

Fig. 5. Results from ISORROPIA II for the 0.6 µm and 3.5 µm size fractions in 2009, and the <0.47 µm and >2.4 µm size fractions in 2010. Model inputs are given in Table 3. The range and mean RH in 2009 and 2010 are indicated next to the horizontal axes.

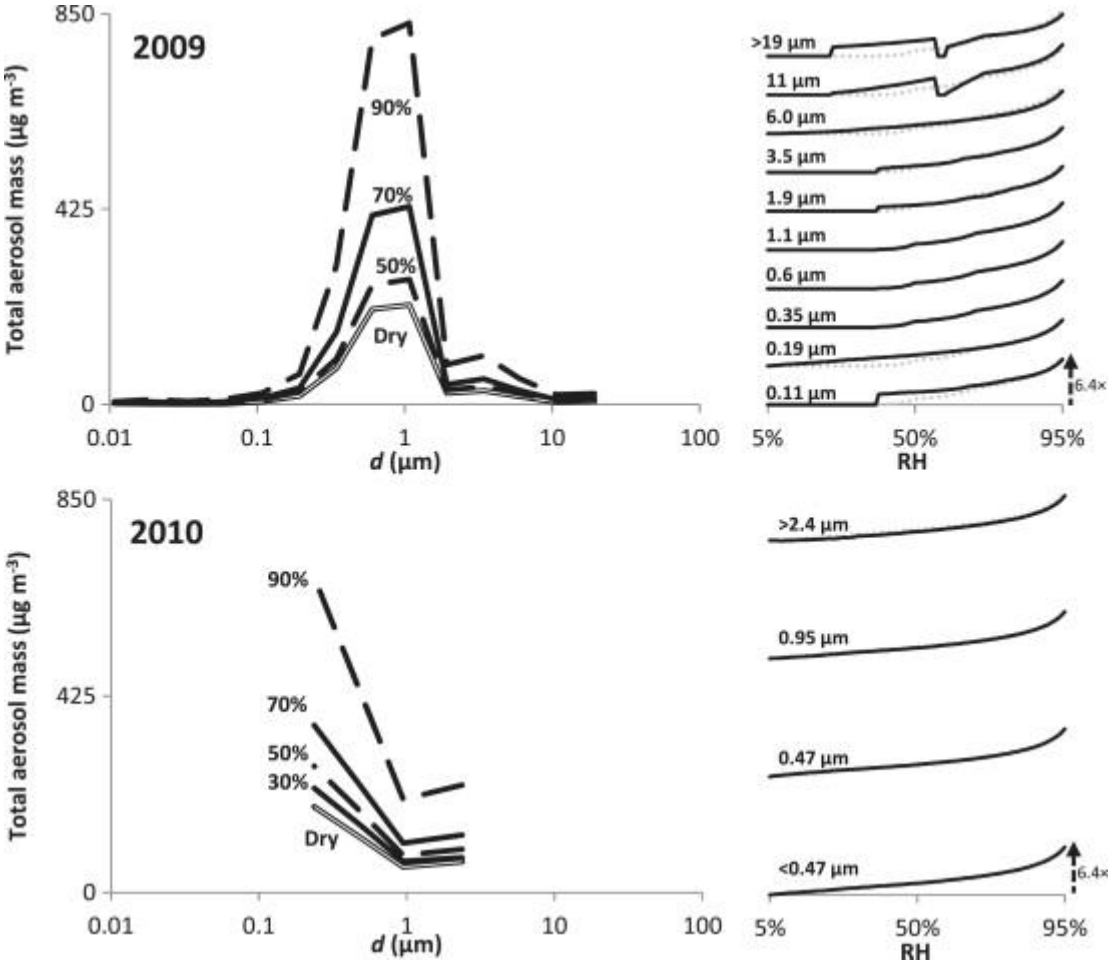

Fig. 6. Results from ISORROPIA II showing total aerosol mass in each size fraction (µg m^{-3}) in 2009 and 2010 at varying RH and 35 °C. Also shown is the sensitivity of total aerosol mass in each size fraction to RH, compared to the sensitivity in the 0.6 µm fraction in 2009 and the <0.47 µm fraction in 2010 (the vertical axes are logarithmic).

Appendix 1.

Composition-resolved size distributions of Masaya's volcanic aerosol in 2007, 2009 and 2010. Concentrations of ions are given in μmol m^{-3}.

Sample	*d*/μm	SO_4^{2-}	Cl^-	F^-	NO_3^-	Na^+	K^+	Mg^{2+}	Ca^{2+}	NH_4^+
	>19	0.015	0	0	0	–	–	–	–	–
	11	0.012	0.00049	0.035	0	–	–	–	–	–
	6	0.09	0.0035	0.02	0.066	–	–	–	–	–
	3.5	0.35	0.0029	0.0048	0	–	–	–	–	–
	1.9	0.3	0.0014	0.0041	0.028	–	–	–	–	–
	1.1	0.23	0.0003	0	0	–	–	–	–	–
	0.6	0.81	0	0	0	–	–	–	–	–
7/1	0.35	1.9	0	0	0	–	–	–	–	–
	0.19	1.7	0	0	0	–	–	–	–	–
	0.11	0.6	0	0	0	–	–	–	–	–
	0.06	0.031	0	0	0	–	–	–	–	–
	0.035	0.0047	0	0	0	–	–	–	–	–
	0.019	0.0022	0	0	0	–	–	–	–	–
	0.011	0.0015	0	0	0	–	–	–	–	–
	>19	0.0097	0.0072	0	0	–	–	–	–	–
	11	0.029	0.019	0	0	–	–	–	–	–
	6	0.066	0.02	0.0032	0	–	–	–	–	–
7/2	3.5	0.13	0.025	0.0025	0	–	–	–	–	–
	1.9	0.3	0.017	0.00027	0	–	–	–	–	–
	1.1	0.24	0.022	0	0	–	–	–	–	–
	0.6	1.6	0.0066	0	0	–	–	–	–	–

Sample	*d*/μm	SO_4^{2-}	Cl^-	F^-	NO_3^-	Na^+	K^+	Mg^{2+}	Ca^{2+}	NH_4^+
	0.35	0.83	0.0066	0	0	–	–	–	–	–
	0.19	0.67	0.0068	0	0	–	–	–	–	–
	0.11	0.25	0.0052	0	0	–	–	–	–	–
	0.06	0.028	0.0038	0	0	–	–	–	–	–
	0.035	0.0071	0.011	0	0	–	–	–	–	–
	0.019	0.0026	0.006	0	0	–	–	–	–	–
	0.011	0	0.0058	0	0	–	–	–	–	–
	>19	0.0059	0.00097	0.0054	0	–	–	–	–	–
	11	0.003	0	0	0	–	–	–	–	–
	6	0.0031	0.0018	0	0	–	–	–	–	–
	3.5	0.0025	0.002	0	0	–	–	–	–	–
	1.9	0.006	0.0037	0	0	–	–	–	–	–
	1.1	0.0059	0.0056	0	0	–	–	–	–	–
	0.6	0.095	0.00034	0	0	–	–	–	–	–
7/3	0.35	0.18	0	0	0	–	–	–	–	–
	0.19	0.094	0	0	0	–	–	–	–	–
	0.11	0.032	0	0	0	–	–	–	–	–
	0.06	0.0098	0.0018	0.012	0	–	–	–	–	–
	0.035	0.0021	0	0	0	–	–	–	–	–
	0.019	0.0044	0	0.0023	0	–	–	–	–	–
	0.011	0.0086	0	0	0	–	–	–	–	–
	>19	0.47	0	0	0	–	–	–	–	–
7/4	11	0.037	0.022	0.013	0	–	–	–	–	–
	6	0.2	0.01	0.025	0	–	–	–	–	–

Sample	*d*/μm	SO_4^{2-}	Cl^-	F^-	NO_3^-	Na^+	K^+	Mg^{2+}	Ca^{2+}	NH_4^+
	3.5	0.45	0	0.1	0	–	–	–	–	–
	1.9	0.24	0.00037	0.062	0	–	–	–	–	–
	1.1	0.27	0	0.0073	0	–	–	–	–	–
	0.6	0.75	0	0	0	–	–	–	–	–
	0.35	2.4	0	0	0	–	–	–	–	–
	0.19	1.6	0.00084	0	0	–	–	–	–	–
	0.11	0.31	0.0074	0	0	–	–	–	–	–
	0.06	0.038	0.11	0	0	–	–	–	–	–
	0.035	0.0086	0.0046	0.027	0	–	–	–	–	–
	0.019	0.0015	0.0036	0.023	0	–	–	–	–	–
	0.011	0.0027	0.005	0	0	–	–	–	–	–
	>19	0.0054	0.0059	0.0041	0	–	–	–	–	–
	11	0.0099	0.012	0.0082	0	–	–	–	–	–
	6	0.022	0.038	0.00035	0	–	–	–	–	–
	3.5	0.049	0.014	0	0	–	–	–	–	–
	1.9	0.064	0.0061	0	0	–	–	–	–	–
	1.1	0.081	0	0	0	–	–	–	–	–
7/5	0.6	0.77	0.00065	0	0	–	–	–	–	–
	0.35	1.6	0.00065	0	0	–	–	–	–	–
	0.19	0.6	0.0011	0	0	–	–	–	–	–
	0.11	0.079	0	0	0	–	–	–	–	–
	0.06	0.0083	0.0049	0	0	–	–	–	–	–
	0.035	0.0039	0.00015	0	0	–	–	–	–	–
	0.019	0.0016	0.0016	0	0	–	–	–	–	–

Sample	*d*/μm	SO_4^{2-}	Cl^-	F^-	NO_3^-	Na^+	K^+	Mg^{2+}	Ca^{2+}	NH_4^+
	0.011	0.00022	0.00089	0	0	–	–	–	–	–
	>19	0.018	0.055	0	0	–	–	–	–	–
	11	0.019	0.042	0	0	–	–	–	–	–
	6	0.07	0.056	0	0	–	–	–	–	–
	3.5	0.2	0.03	0.00063	0	–	–	–	–	–
	1.9	0.24	0.043	0.0023	0	–	–	–	–	–
	1.1	0.18	0.011	0	0	–	–	–	–	–
	0.6	1.8	0.0061	0	0	–	–	–	–	–
7/6	0.35	0.93	0.016	0	0	–	–	–	–	–
	0.19	0.66	0.027	0	0	–	–	–	–	–
	0.11	0.12	0.016	0	0	–	–	–	–	–
	0.06	0.04	0.01	0	0	–	–	–	–	–
	0.035	0.0034	0.0098	0	0	–	–	–	–	–
	0.019	0.0062	0.011	0	0	–	–	–	–	–
	0.011	0.0052	0.0098	0	0	–	–	–	–	–
	>19	0.0023	0.0043	0	0	–	–	–	–	–
	11	0.03	0.0079	0	0	–	–	–	–	–
	6	0.016	0.011	0	0	–	–	–	–	–
	3.5	0.041	0.028	0	0	–	–	–	–	–
7/7	1.9	0.065	0.024	0	0	–	–	–	–	–
	1.1	0.077	0.025	0	0	–	–	–	–	–
	0.6	0.084	0.012	0	0	–	–	–	–	–
	0.35	0.96	0.0015	0	0	–	–	–	–	–
	0.19	0.87	0.0039	0	0	–	–	–	–	–

Sample	*d*/μm	SO_4^{2-}	Cl^-	F^-	NO_3^-	Na^+	K^+	Mg^{2+}	Ca^{2+}	NH_4^+
	0.11	0.67	0.0037	0	0	–	–	–	–	–
	0.06	0.087	0.0013	0	0	–	–	–	–	–
	0.035	0.0086	0.0029	0	0	–	–	–	–	–
	0.019	0.0013	0.0011	0	0	–	–	–	–	–
	0.011	0.00097	0.0025	0	0	–	–	–	–	–
	>19	0	0.003	0	0	–	–	–	–	–
	11	0.012	0.011	0.017	0	–	–	–	–	–
	6	0.01	0.0086	0.015	0	–	–	–	–	–
	3.5	0.024	0.076	0.016	0	–	–	–	–	–
	1.9	0.03	0.22	0.021	0.02	–	–	–	–	–
	1.1	0.018	0.11	0.014	0.011	–	–	–	–	–
	0.6	0.036	0.078	0.013	0.0079	–	–	–	–	–
7/8	0.35	0.0098	0.007	0.0092	0	–	–	–	–	–
	0.19	0.012	0.0024	0.0084	0	–	–	–	–	–
	0.11	0.012	0.017	0.029	0	–	–	–	–	–
	0.06	0.055	0.0036	0.0018	0	–	–	–	–	–
	0.035	0.019	0.00054	0.0049	0	–	–	–	–	–
	0.019	0.02	0.031	0.036	0.0086	–	–	–	–	–
	0.011	0.016	0.016	0.0053	0	–	–	–	–	–
	>19	0.029	0.0059	0.0079	0	–	–	–	–	–
	11	0.013	0.046	0.029	0	–	–	–	–	–
7/9	6	0.0025	0.033	0.0055	0	–	–	–	–	–
	3.5	0.016	0.16	0.0073	0.082	–	–	–	–	–
	1.9	0.017	0.12	0.0055	0.13	–	–	–	–	–

Sample	*d*/μm	SO_4^{2-}	Cl^-	F^-	NO_3^-	Na^+	K^+	Mg^{2+}	Ca^{2+}	NH_4^+
	1.1	0.019	0.1	0.0055	0.14	–	–	–	–	–
	0.6	0.013	0.039	0.0067	0.044	–	–	–	–	–
	0.35	0.057	0.0079	0.0073	0	–	–	–	–	–
	0.19	0.057	0.022	0.045	0	–	–	–	–	–
	0.11	0.028	0.0059	0.0086	0	–	–	–	–	–
	0.06	0.022	0.0065	0.022	0	–	–	–	–	–
	0.035	0.0089	0.00053	0.0048	0	–	–	–	–	–
	0.019	0.0052	0.0012	0.0042	0	–	–	–	–	–
	0.011	0.0033	0.0015	0.0048	0	–	–	–	–	–
	>19	0.0017	0	0.0014	0	–	–	–	–	–
	11	0.006	0.021	0.013	0	–	–	–	–	–
	6	0.0012	0.015	0.0026	0	–	–	–	–	–
	3.5	0.0075	0.074	0.0034	0.039	–	–	–	–	–
	1.9	0.008	0.054	0.0026	0.059	–	–	–	–	–
	1.1	0.009	0.049	0.0026	0.068	–	–	–	–	–
	0.6	0.0062	0.018	0.0031	0.02	–	–	–	–	–
7/10	0.35	0.027	0.0037	0.0034	0	–	–	–	–	–
	0.19	0.027	0.01	0.021	0	–	–	–	–	–
	0.11	0.013	0.0028	0.004	0	–	–	–	–	–
	0.06	0.01	0.0031	0.01	0	–	–	–	–	–
	0.035	0.0042	0.00025	0.0023	0	–	–	–	–	–
	0.019	0.0025	0.00056	0.002	0	–	–	–	–	–
	0.011	0.0015	0.00072	0.0023	0	–	–	–	–	–
9/1	>19	0.0054	0.013	0	0	0.0013	0.0036	0.00086	0.0054	0

Sample	*d*/μm	SO_4^{2-}	Cl^-	F^-	NO_3^-	Na^+	K^+	Mg^{2+}	Ca^{2+}	NH_4^+
	11	0.0089	0.028	0	0	0.018	0.0046	0.00072	0.0042	0
	6	0.025	0.021	0	0	0.026	0.0094	0.002	0.0057	0
	3.5	0.048	0.025	0	0	0.058	0.02	0.0047	0.011	0
	1.9	0.065	0.014	0	0	0.063	0.026	0.0037	0.0064	0
	1.1	0.37	0	0	0	0.27	0.16	0.003	0.0066	0
	0.6	0.35	0	0	0	0.27	0.2	0.0033	0.0022	0
	0.35	0.22	0	0	0	0.17	0.11	0.0014	0.00082	0
	0.19	0	0	0	0	0	0	0	0.0017	0
	0.11	0.035	0	0	0	0.025	0.016	0.00072	0.00069	0
	0.06	0	0	0	0	0.0032	0.0031	0.0003	0.003	0
	0.035	0	0	0	0	0.0028	0.0024	0.00064	0.00087	0
	0.019	0	0	0	0	0.0035	0.0024	0.00077	0.00083	0
	0.011	0	0	0	0	0.0032	0.0026	0.0003	0.0021	0
	>19	0.021	0	0.025	0	0.017	0.0082	0.0023	0.0078	0
	11	0.022	0	0.013	0	0.015	0.0078	0.0012	0.0053	0
	6	0.041	0	0	0	0.034	0.015	0	0.012	0
	3.5	0.086	0.01	0	0	0.081	0.037	0.0046	0.012	0
	1.9	0.089	0	0.026	0	0.072	0.035	0.0036	0.0072	0
9/2	1.1	0.43	0	0	0	0.29	0.19	0.0023	0.0039	0
	0.6	0.5	0	0	0	0.26	0.4	0.0012	0.0022	0
	0.35	0.16	0	0	0	0.12	0.076	0.0031	0.0064	0
	0.19	0.044	0	0	0	0.028	0.017	0	0.001	0
	0.11	0.01	0.0099	0	0	0.0075	0.0051	0.00038	0.006	0
	0.06	0	0	0	0	0.002	0.0027	0.0014	0.0051	0

Sample	*d*/μm	SO_4^{2-}	Cl^-	F^-	NO_3^-	Na^+	K^+	Mg^{2+}	Ca^{2+}	NH_4^+
	0.035	0	0	0	0	0.0029	0.0022	0.00066	0.00084	0
	0.019	0	0	0	0	0.0038	0.0024	0.00041	0.0043	0
	0.011	0	0	0	0	0.0023	0.0022	0.00038	0.0032	0
	>19	0.053	0	0	0	0.011	0.0061	0.00087	0.0052	0
	11	0.0077	0.049	0	0	0.053	0.0058	0.00066	0.0028	0
	6	0.14	0	0.016	0	0.026	0.011	0.0022	0.0054	0
	3.5	0.067	0	0	0	0.062	0.027	0.0049	0.011	0
	1.9	0.094	0	0	0	0.081	0.04	0.0051	0.0094	0
	1.1	0.59	0	0	0	0.36	0.23	0.0039	0.0053	0
	0.6	0.93	0	0	0	0.54	0.64	0.00087	0.0018	0
9/3	0.35	0.13	0	0	0	0.098	0.064	0	0.00083	0
	0.19	0.12	0	0	0	0.03	0.019	0	0.0036	0
	0.11	0.0082	0.02	0	0	0.0074	0.006	0.0011	0.0071	0
	0.06	0	0	0	0	0.0019	0.0037	0.00043	0.000013	0
	0.035	0	0	0	0	0.0019	0.0031	0.00055	0	0
	0.019	0	0	0	0	0.0044	0.0032	0.0027	0.0052	0
	0.011	0	0	0	0	0	0	0.00043	0	0
	>19	0	0	0	0	0.053	0.013	0.026	0.056	0
	11	0	0	0	0	0.008	0.0043	0.00076	0.0022	0
	6	0.057	0	0	0	0.016	0.007	0.0025	0.0049	0
9/4	3.5	0.13	0	0	0	0.037	0.016	0.0029	0.0072	0
	1.9	0.044	0	0	0	0.049	0.024	0.0039	0.0063	0
	1.1	0.44	0	0	0	0.25	0.15	0.0028	0.0045	0
	0.6	0.58	0	0	0	0.3	0.36	0.00045	0.0018	0

Sample	*d*/μm	SO_4^{2-}	Cl^-	F^-	NO_3^-	Na^+	K^+	Mg^{2+}	Ca^{2+}	NH_4^+
	0.35	0.12	0	0	0	0.037	0.023	0	0.00054	0
	0.19	0.13	0	0	0	0.017	0.011	0.00073	0.0025	0
	0.11	0.014	0.13	0	0	0.011	0.0041	0	0.00049	0
	0.06	0	0	0	0	0.0047	0.0059	0.00071	0.0026	0
	0.035	0.0013	0	0	0	0.0047	0.0031	0	0.0013	0
	0.019	0.001	0	0	0	0.0025	0.003	0.00034	0.00042	0
	0.011	0.036	0	0	0	0.0029	0.003	0.00037	0.0013	0
	>19	0.042	0	0	0	0.012	0.0045	0.0037	0.0055	0
	11	0.041	0	0	0	0.006	0.003	0.0007	0.0012	0
	6	0.04	0	0	0	0.006	0.0029	0.00067	0	0
	3.5	0.0012	0.022	0	0	0.017	0.003	0.0028	0.00067	0
	1.9	0	0.026	0	0	0.022	0.0041	0.0045	0.0062	0
	1.1	0	0.018	0	0	0.017	0.0036	0.002	0.00079	0
	0.6	0.08	0	0	0	0.066	0.036	0.00077	0.0014	0
9/5	0.35	0.042	0	0	0	0.0021	0.003	0.0014	0.001	0
	0.19	0.041	0	0	0	0.0026	0.0039	0.0004	0.0009	0
	0.11	0.067	0.66	0	0	0.0099	0.0083	0.00067	0.00079	0
	0.06	0.0015	0	0	0	0.0047	0.0029	0.00084	0.0015	0
	0.035	0.041	0	0	0	0.003	0.0032	0.00064	0.0028	0
	0.019	0	0	0	0	0.003	0.022	0	0.0018	0
	0.011	0	0	0	0	0.0064	0.019	0.0006	0.00086	0
	>2.4	0.072	0.017	0	0	0.046	0.011	0.006	0.0078	0
10/1	0.95	0.073	0	0	0	0.035	0.0065	0.0041	0	0
	0.47	0.11	0	0	0	0.024	0.01	0.00082	0	0

Sample	*d*/μm	SO_4^{2-}	Cl^-	F^-	NO_3^-	Na^+	K^+	Mg^{2+}	Ca^{2+}	NH_4^+
	<0.47	0.23	0.012	0	0	0.059	0.035	0.0016	0	0
	>2.4	0.17	0	0	0	0.1	0.021	0.014	0	0
	0.95	0.18	0	0	0	0.061	0.013	0.0062	0	0
10/2										
	0.47	0.27	0	0	0	0.044	0.02	0.00097	0	0
	<0.47	0.28	0	0	0	0.066	0.037	0.0002	0	0
	>2.4	0.31	0	0	0	0.12	0.068	0.017	0	0
	0.95	0.19	0	0	0	0.058	0.034	0.0062	0	0
10/3										
	0.47	0.67	0	0	0	0.11	0.068	0.00065	0	0
	0.1	1.1	0.014	0	0	0.31	0.19	0.00031	0	0
	>2.4	0	0.061	0	0	0.034	0.0038	0.003	0	0
	0.95	0	0	0	0	0.017	0	0.0016	0	0
10/4										
	0.47	0	0	0	0	0.029	0.015	0	0	0
	<0.47	0.0085	0	0	0	0.0014	0.005	0	0	0
	>2.4	0.54	0	0.014	0	0.17	0.079	0.021	0	0
	0.95	0.33	0	0	0	0.084	0.037	0.0069	0	0
10/5										
	0.47	0.98	0	0	0	0.19	0.1	0.00065	0	0
	<0.47	1.8	0	0	0	0.49	0.28	0.00063	0	0